Received: 16 January 2023 | Revised: 21 June 2023 | Accepted: 25 July 2023

DOI: 10.1002/rob.22239

RESEARCH ARTICLE

WILEY

Modeling of flexible metal wheel for pressurized lunar rover and traction performance prediction

Jianzhong Zhu[1,2,3] | Yan Shen[3] | Pujun Hao[1,2] | Jingna Liu[1,2] | Yuqiong Li[4,5] | Kang Wang[6] | Meng Zou[3]

[1]Tianjin Key Laboratory for Advanced Mechatronic System Design and Intelligent Control, School of Mechanical Engineering, Tianjin University of Technology, Tianjin, China

[2]National Demonstration Center for Experimental Mechanical and Electrical Engineering Education, Tianjin University of Technology, Tianjin, China

[3]Key Laboratory for Bionics Engineering of Education Ministry, Jilin University, Changchun, China

[4]Key Laboratory for Mechanics in Fluid Solid Coupling Systems, Institute of Mechanics, Chinese Academy of Sciences, Beijing, China

[5]Guangdong Aerospace Research Academy, Guangdong, China

[6]Institute of Spacecraft System Engineering CAST, Beijing, China

Correspondence

Yuqiong Li, Key Laboratory for Mechanics in Fluid Solid Coupling Systems, Institute of Mechanics, Chinese Academy of Sciences, 100190 Beijing, China.
Email: liyuqiong@imech.ac.cn

Funding information

Experiments for Space Exploration Program; Guangdong Aerospace Research Academy Research Project; National Natural Science Foundation of China; China Academy of Space Technology, Grant/Award Number: TKTSPY-2020-05-01; Youth Innovation Promotion Association of the Chinese Academy of Sciences, Grant/Award Number: Y2022009

Abstract

The pressurized lunar rover has become one of the most important equipment in lunar exploration and resource utilization missions. On the terrain of soft lunar regolith, the rover wheels are easy to slip, sink, or even fail to move. To improve the traction performance of the rover on soft lunar soil, it is necessary to study the interaction between the wheels and the lunar soil. The deformation of the flexible wheel provides a larger contact area, which results in greater tractive force. Moreover, flexible wheels have better comfort and stability than rigid wheels, which are needed for manned rovers. However, there are few studies on the wheel soil interaction model of the heavy flexible wheel for the pressurized lunar rover. In this paper, a metal flexible wheel soil interaction model for pressurized lunar rovers was established, and the traction performance of the flexible wheel was predicted by using this model. Then, the accuracy of the wheel soil interaction model was verified by the soil bin test. The experimental results showed that the average error between the theoretical value of sinkage and the experimental value was 13.9%, and the average error between the theoretical and experimental value of drawbar pull was 11.5%, indicating that the model has high prediction accuracy. The new model can be used to predict the traction performance of flexible wheels and the experimental results can provide a reference for the flexible wheel design lunar rovers.

KEYWORDS

flexible metal wheel, pressurized lunar rover, traction performance, wheel soil interaction model

1 | INTRODUCTION

Since the official launch of the "Chang'e Project" lunar exploration program in 2004, China has completed the three-stage goals of "circling, landing, and returning" in 2020, and plans to achieve a manned lunar landing around 2030 and establish a scientific research station (Li et al., 2019). The pressurized lunar rover can not only carry a large number of scientific exploration instruments but also provide space for astronauts to stay on the lunar surface. It has become one of the most important equipment in lunar exploration and resource utilization missions.

The wheeled mobile system has been widely used in the field of planetary exploration due to its advantages of mature technology and high reliability (Gromov et al., 2003; Kwan, 2021; Reeves & Neilson, 2005; Squyres, 2005; Wan et al., 2020). As a part of direct contact with the lunar soil, the wheel plays the role of support, drive,

steering, and braking, which determines the mobility, ride comfort, stability, and safety of the lunar rover.

The lunar surface is covered with one layer of soft lunar regolith. On such soft terrain, the rover wheels are easy to slip, sink, or even fail to move. Therefore, to better understand the traction performance of the rover on soft lunar soil, it is necessary to study the interaction between the wheels and the lunar soil.

The interaction between wheel and soil has been extensively studied, and Bekker's pressure sinkage model has been widely used (Bekker, 1956, 1960, 1969). Wong and Reece (1967a, 1967b) established two comprehensive frameworks for predicting the performance of driven and towed rigid wheels, and the effect of slip on sinkage, motion resistance, and thrust, have been taken into account. Soil shear strength is another important factor affecting vehicle traction performance. Bekker proposed an equation to describe the shear stress of brittle soil, while Janosi (1961) thought that the most common ground was plastic ground and proposed a formula for calculating the shear stress for plastic ground. Recently, these terramechanics-based wheel soil interaction models have been successfully applied to the traction performance analysis of planetary rovers (Ding et al., 2015; Huang et al., 2019; Jiang et al., 2017; Sutoh et al., 2012). Irani et al. (2011) present a validated dynamic terramechanics model for rigid wheels with grousers that may be used for planetary and terrestrial mobile robots operating in loose sandy soil. Huang et al. (2018) analyzed the main parameters of the wheel–soil interaction model and studied the sinkage characteristics of the rover based on the similarity theory. Guo et al. (2020) proposed a wheel–terrain model for high-slip scenarios that can be used to estimate wheel traveling performance accurately.

With the rise of manned detection, people pay more and more attention to the flexible wheels suitable for manned detection vehicles. As the only manned rover to land on the moon, the lunar roving vehicle uses flexible wire mesh wheels. The analysis results indicate that wheel deformation significantly benefits slope climbing ability (Asnani et al., 2009). Favaedi et al. (2011) present a new model that characterizes the traction performance of metal flexible wheels operating on deformable terrain. The flexible wheel provides a larger contact area due to the deformation of the wheel which results in greater tractive force. Iizuka and Kubota (2011) designed a small flexible wheel made of beryllium copper, and the test results showed that the flexible wheel showed high performance for traversing loose terrain. Sharma et al. (2018) formulated a methodology to systematically design a flexible wheel for a low-mass lunar rover, and the average ground pressure and the substitution circle equation are used to calculate the wheel stiffness. Wang et al. (2019) assumed that the deformation of the elastic wheel was elliptic and established a wheel–soil interaction model of the elastic wheel according to the geometric relationship. The existing research mainly focuses on small planetary wheels, while there are few studies on heavy manned lunar rover wheels, especially the flexible wheels suitable for the pressurized lunar rover, which are urgently needed for China's lunar exploration in the next stage. In addition, the existing mathematical model is not suitable for discrete twin wheel carcasses, so it is urgent to develop a new flexible wheel–soil interaction model.

In the early stage of this project, a metal flexible wheel has been developed and its bearing capacity has been tested (Zou et al., 2020). On the basis of the theory of terramechanics and the load–deformation relationship of flexible wheels, a static wheel soil interaction model is established in this paper, and an iterative method is used to solve the static sinkage and entry angle. Furthermore, the dynamic interaction model was established, including sinkage, bulldozing resistance, compaction resistance, and drawbar pull. Then, a soil bin test system is developed to verify the accuracy of the mathematical model established. Finally, the traction performance of the flexible wheel is predicted by the mathematical model.

2 | WHEEL–SOIL INTERACTION MODEL

2.1 | Static wheel–soil interaction

2.1.1 | Geometric deformation analysis of flexible wheel

Under the action of vertical load, elastic deformation will occur on the surface of the flexible wheel surface, which leads to the interaction between the flexible wheel and the lunar soil being different from that of the rigid wheel. Figure 1 shows the interaction

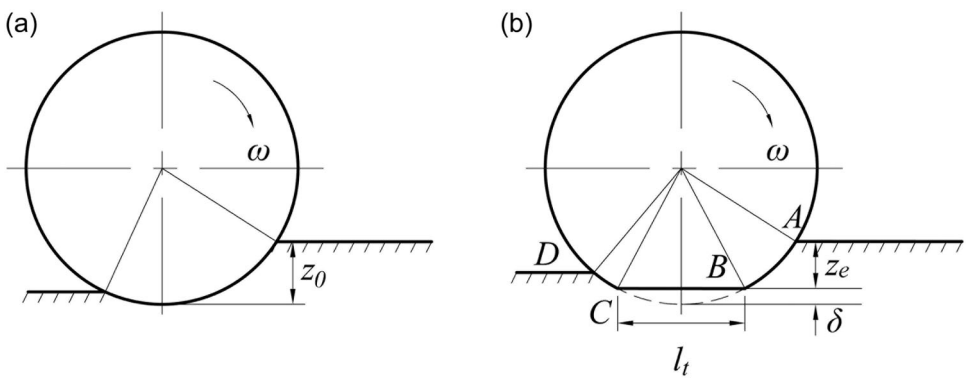

FIGURE 1 Interaction between wheel and lunar soil. (a) Rigid wheel and (b) flexible wheel.

relationship between wheels and lunar soil. It can be found that the rigid wheel has no obvious deformation, while the flexible wheel surface will undergo significant deformation, which is obviously different from the rigid wheel. In the wheel soil interaction model, the reaction force from the ground to the rigid wheel is purely radial. For flexible wheels, due to wheel surface deformation, the wheel soil contact area is divided into three distinct segments: *AB*, *BC*, and *CD* segments. It is assumed that *AB* and *CD* segments are not deformed, and are still circular arcs, and the *BC* segment is flattened.

2.1.2 | Flexible wheel design

As shown in Figure 2, the main structure of the metal flexible wheel includes elastic wheel carcasses, rigid rim, and tread strips. For the manned lunar rover, stiffness and strength shall be taken into account when designing flexible wheels. To improve the load capacity and reliability of the wheel, an innovative type of flexible metal wheel consisting of a single rim and twin carcasses was developed (Zou et al., 2020). Compared with the single-wheel structure, the twin-carcasses structure can not only disperse the forces on the wheel surface, but also reduce the risk of wheel failure caused by partial deformation or damage of the carcasses. The hollow-out rim structure is designed to meet the requirements of strength and reduce the mass of the wheel. To improve the traction performance of wheels on soft lunar soil, most wheels are designed with lugs or tread (Inotsume et al., 2019; Lakdawalla, 2018; Sharma et al., 2018; Sutoh et al., 2013; Wiberg et al., 2021). Considering the speed of the pressurized lunar rover, the special discrete wheel surface structure of the flexible wheel, and the influence of the tread strips on the ride performance, this study designed an X-shape wheel tread with a thickness of 1.5 mm. The whole wheel contains 36 strips, which are overlapped by each other and connected to the wheel carcasses through bolts.

The flexible wheel will deform during running, which will affect the interaction between the wheel and soil. The study of deformation characteristics of the metal flexible wheel is the basis of wheel soil interaction modeling. The load–deformation curve (Figure 3) and the load–deformation equation of the flexible wheel are obtained by polynomial fitting using the vertical load–deformation test data of the flexible wheel:

$$W_1 = 178.21\delta + 4187.66\delta^2, \quad (1)$$

where W_1 is the vertical load and δ is the deformation of the flexible wheel.

2.1.3 | Mathematical model of static interaction

At a static state, the flexible wheel reached mechanical equilibrium under the action of load on the wheel and vertical supporting force of lunar soil, as shown in Figure 4. It can be seen from the figure that the flexible wheel produces elastic deformation δ due to the load W on the wheel, and produces a sinkage z_e in the lunar soil, while the vertical reaction force F_z generated by the lunar soil is balanced with the wheel load W. F_z consists of three parts, including (1) the supporting force F_1 of lunar soil on the undeformed part *AB* of the flexible wheel, (2) the vertical reaction force F_c of the flattening segment *BC*, and (3) the supporting force F_2 of the undeformed part *CD*. Since the *CD* segment is symmetric to the *AB* segment, F_2 is equal to F_1, and the vertical reaction force of lunar soil can be expressed as follows:

$$F_z = F_1 + F_c + F_2 = 2F_1 + F_c, \quad (2)$$

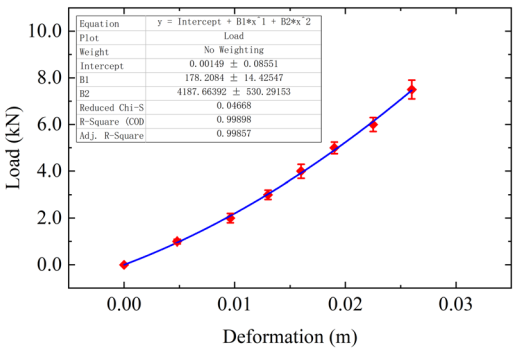

FIGURE 3 Load–deformation fitting curve.

FIGURE 2 Flexible metal wheel.

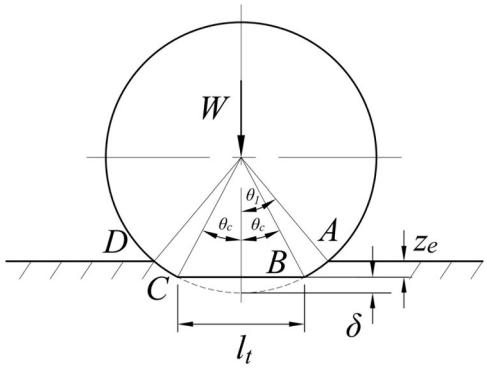

FIGURE 4 Static wheel soil interaction.

where F_c is equal to the load W_1 when the deformation of the flexible wheel is δ on the load test machine:

$$F_c = W_1. \tag{3}$$

When the rubber pneumatic tire deforms under load, the relationship between the sinkage and the ground pressure can be described by the carcass stiffness p_c and the inflation pressure p_i. However, the pressure p_c exerted on the terrain due to the carcass stiffness is difficult to determine, as it varies with the inflation pressure and normal load of the tire. As an alternative, Bekker proposed to use the average ground pressure P_g of a tire on hard ground to represent the sum of p_i and p_c. The average ground pressure P_g is equal to the load W carried by the tire divided by the ground contact area (Wong, 2009). Drawing on this idea, the static sinkage of the flexible wheel on soft ground in this study can be expressed as

$$z_e = \left(\frac{P_g}{k_c/B + k_\phi}\right)^{\frac{1}{n}}, \tag{4}$$

where the average ground pressure P_g can be calculated by the ratio of the load on the flattening segment BC to the ground area:

$$P_g = \frac{W_1}{l_t \times B}, \tag{5}$$

where l_t is the length of the flattening segment BC of the flexible wheel, and B is the width of the flexible wheel. Because the contact area of the discrete wheel carcasses is smaller than that of the continuous wheel carcasses, the calculation results of the model are not accurate. Therefore, the width B was modified to the equivalent width B^* (see Figure 5):

$$B^* = \lambda B, \tag{6}$$

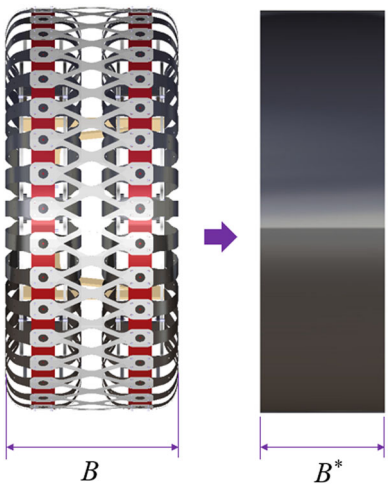

FIGURE 5 Diagram of the equivalent width of flexible wheel.

where the equivalent coefficient $\lambda = 0.75$.

According to the geometric relationship in Figure 4, the l_t can be expressed as

$$l_t = 2\sqrt{r^2 - (r - \delta)^2} = 2\sqrt{2r\delta - \delta^2}. \tag{7}$$

According to Bekker's equation, the radial stress is replaced by the normal stress of the pressing plate at the same depth. Then, according to the geometric relationship of the interaction between soil and wheel, the normal stress along the circular section AB of the wheel can be expressed as

$$\sigma_1(\theta) = \left(\frac{k_c}{B} + k_\phi\right) r^n (\cos\theta - \cos\theta_1)^n \quad (\theta_c \le \theta \le \theta_1), \tag{8}$$

where θ_1 is the entry angle of the flexible wheel, θ_c is the angle corresponding to the half of the flattening section, which can be expressed as follows according to the geometric relationship shown in Figure 4:

$$\theta_1 = arc\cos\left(\frac{r - \delta - z_e}{r}\right), \tag{9}$$

$$\theta_c = arc\cos\left(\frac{r - \delta}{r}\right). \tag{10}$$

Considering the force balance of the flexible wheel in the vertical direction, the normal stress of the arc AB is integrated along the vertical component, and then the supporting force F_1 of this part of lunar soil on the flexible wheel can be obtained.

$$F_1 = B\int_{\theta_c}^{\theta_1} \sigma_1(\theta)\cos(\theta) r\, d\theta = B\left(\frac{k_c}{B} + k_\phi\right) r^n \int_{\theta_c}^{\theta_1} (\cos\theta - \cos\theta_1)^n d\theta \quad \left(\theta_c \le \theta \le \theta_1\right). \tag{11}$$

2.1.4 | Static interaction model solving

In the above static sinkage model, only the parameters of the lunar soil simulant, the wheel load W, and the load–deformation equation of the flexible wheel are known, and there is an integral model, so the explicit solution cannot be obtained directly. Therefore, a numerical iterative method is proposed to solve the static sinkage and entry angle, and the solution process is shown in Figure 6. First, the dimension of the flexible wheel, the wheel load, and the mechanical parameters of the lunar soil simulant were read, and the initial value of δ was given, which was substituted into Equations (1) and (7) to obtain W_1 and l_t. Then, substitute W_1 and l_t into Equations (4) and (5) to obtain z_e, further obtain θ_1 and θ_c, and use Equation (11) to obtain F_1. Finally, Equation (2) was used to obtain F_z. If F_z is equal to W, the value of δ is correct, and then output z_e. If F_z is not equal to W, give a different value of δ again and repeat the process until the correct δ is found.

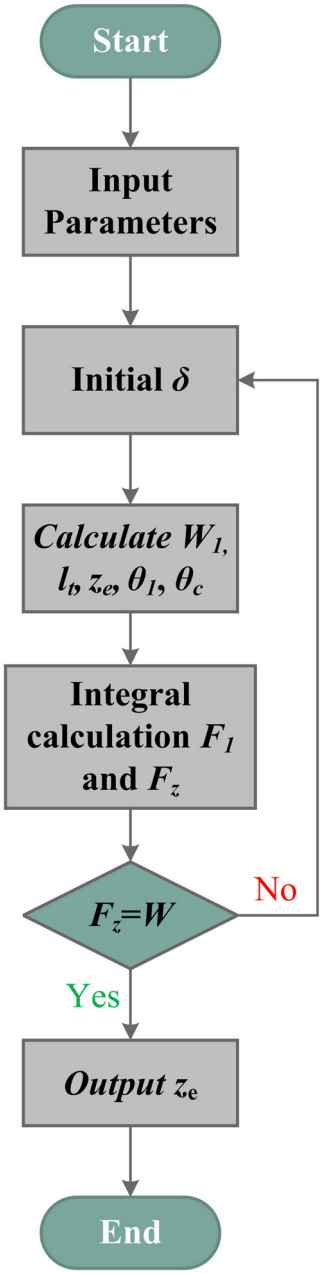

FIGURE 6 Solving process of static sinkage model.

2.2 | Dynamic wheel–soil interaction

The interaction between the wheel and lunar soil is more complex in the operation state than in the static state. The longitudinal flow of the lunar soil is different under different driving conditions and slip ratios. Figure 7 shows the flow pattern of the lunar soil under the wheel when the lunar rover is driven. As can be seen from the figure, the flow of the lunar soil can be divided into two regions: the lunar soil particles in the *ABC* region flow forward due to the push of the wheel, while the lunar soil particles in the *AED* region move downward and backward due to the wheel rotation shear, resulting in wheel sinkage.

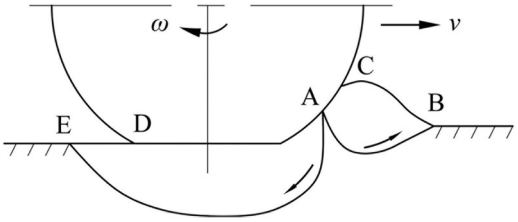

FIGURE 7 Flow pattern of lunar soil under the wheel.

2.2.1 | Dynamic interaction model between the flexible wheel and lunar soil

The sinkage is directly related to the entry angle of the wheel. If the sinkage cannot be accurately predicted, it is impossible to obtain the rolling resistance, thrust, drawbar pull, torque, and so forth.

The increase in cutting lunar soil caused by wheel slip will lead to an increase in wheel sinkage and driving resistance. Therefore, to accurately predict the traction performance of the vehicle, the slip sinkage should be considered. Reece (1964, 1965) believed that soil deformation would cause additional sinkage, and proposed a sinkage calculation formula considering the slip ratio. However, this formula has an obvious defect: when the slip ratio reaches 100%, the sinkage will increase to infinity, and it cannot be tested because it is difficult to distinguish the additional settlement from static sinkage. Lyasko (2010) considered the influence of slip sinkage on the prediction of motion resistance, and derived the slip sinkage formula by using the relationship between the work done by bulldozing force and the work done by compacted soil:

$$z'_e = \frac{1+i}{1-0.5i} \cdot z_e, \tag{12}$$

where i is the slip ratio of the flexible wheel, and z_e is the static sinkage.

The traction performance of the lunar rover depends on two aspects: one is the maximum driving torque provided by the vehicle power system, and the other is the maximum adhesive force of the lunar soil. The smaller one of the two determines the vehicle's traction performance. When the lunar rover's power system can provide enough driving torque to overcome the driving resistance, the maximum adhesive force that the lunar surface can provide to the wheels becomes the limiting factor of the lunar rover's traction performance. It is important to study the interaction between wheel soil and improve the traction performance of the wheel.

Figure 8 shows the interaction model between the flexible wheel and the lunar soil. Similar to the static interaction model, the contact area between the flexible wheel and the lunar soil is also divided into three parts. It is assumed that the *AB* and *CD* sections are circular arcs, and the *BC* section is flattened. The traction performance of the flexible wheel, such as rolling resistance, driving torque, and drawbar pull, can be defined by the normal stress $\sigma(\theta)$ and shear stress $\tau(\theta)$, which change with the angular position θ.

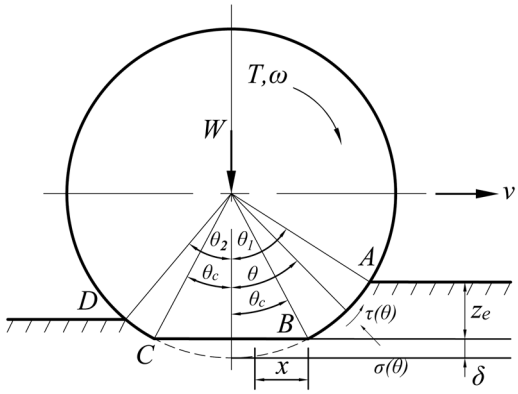

FIGURE 8 Dynamic wheel soil interaction.

According to the geometric relationship in Figure 8, the sinkage at any point of the rim of the flexible wheel can be expressed as

$$z_1 = r(\cos\theta - \cos\theta_1) \quad (\theta_c \le \theta \le \theta_1), \tag{13}$$

$$z_c = r(\cos\theta_c - \cos\theta_1) \quad (-\theta_c \le \theta \le \theta_c), \tag{14}$$

$$z_2 = r(\cos\theta - \cos\theta_2) \quad (-\theta_c \le \theta \le \theta_2). \tag{15}$$

According to Bekker's equation, the normal stress at any point along the rim of the flexible wheel in the circular arc area is equal to the vertical stress under the press plate at the same depth, then the normal stress can be expressed as

$$\sigma_1(\theta) = \left(\frac{k_c}{B} + k_\phi\right)[r(\cos\theta - \cos\theta_1)]^n \quad (\theta_c \le \theta \le \theta_1), \tag{16}$$

$$\sigma_{BC}(\theta) = \left(\frac{k_c}{B} + k_\phi\right)[r(\cos\theta_c - \cos\theta_1)]^n \quad (-\theta_c \le \theta \le \theta_c), \tag{17}$$

$$\sigma_2(\theta) = \left(\frac{k_c}{B} + k_\phi\right)[r(\cos\theta - \cos\theta_2)]^n \quad (-\theta_c \le \theta \le \theta_2). \tag{18}$$

The shear stress generated by the wheel soil interaction is a function of shear displacement. To obtain the shear stress at the contact interface of the soil interaction, it is necessary to analyze the shear displacement along the contact interface. In section *AB*, the shear displacement of lunar soil can be expressed as

$$j_{AB} = r[(\theta_1 - \theta) - (1 - i)(\sin\theta_1 - \sin\theta)], \tag{19}$$

where i is the slip ratio, which can be expressed as

$$i = 1 - \frac{v}{\omega r}, \tag{20}$$

where v is the linear velocity, ω is the angular velocity, and r is the radius of the wheel.

In section *BC*, the slip velocity of the lunar soil is the same. Therefore, the cumulative shear displacement j_x at a distance x from point *B* is then given by

$$j_x = j_B + ix, \tag{21}$$

where j_B is the shear displacement at point *B*.

In section *CD*, the calculation method of lunar soil shear displacement is the same as that in section *AB*.

According to Janosi's shear stress and shear displacement equation (Janosi, 1961), the shear stress distribution in each area of the flexible wheel can be expressed as follows:

$$\tau_1(\theta) = [c + \sigma_1(\theta)\tan\phi]\left(1 - e^{\frac{-j_{AB}}{k}}\right), \tag{22}$$

$$\tau_{BC}(\theta) = [c + \sigma_c(\theta)\tan\phi]\left(1 - e^{\frac{-j_x}{k}}\right), \tag{23}$$

$$\tau_2(\theta) = [c + \sigma_2(\theta)\tan\phi]\left(1 - e^{\frac{-j_{CD}}{k}}\right). \tag{24}$$

Therefore, the wheel load can be expressed as

$$W = B\int_{\theta_c}^{\theta_1}[r(\sigma_1(\theta)\cos\theta + \tau_1(\theta)\sin\theta)]\,d\theta + 2Brp_g\sin\theta_c + B\int_{\theta_2}^{\theta_c}[r(\sigma_2(\theta)\cos\theta + \tau_2(\theta)\sin\theta)]\,d\theta. \tag{25}$$

2.2.2 | Driving resistance

On soft lunar terrain, the wheels are subject to various resistances, thus reducing the trafficability of the lunar rover. When the wheel is driving on the lunar soil, the lunar soil under the wheel will be compacted, and the resulting resistance is called compaction resistance (Poletayev, 1964; Wong & Reece, 1967b). Compaction resistance is the main form of driving resistance when driving on flat and soft terrain.

The compaction resistance of the flexible wheel can be obtained by integrating the horizontal component of the normal stress in the arc sections *AB* and *CD* (Figure 8):

$$R_c = B\int_{\theta_c}^{\theta_1} r\sigma_1(\theta)\sin\theta\,d\theta - B\int_{\theta_c}^{\theta_2} r\sigma_2(\theta)\sin\theta\,d\theta. \tag{26}$$

As can be seen in Figure 8, the normal stress of the flattening section *BC* has no horizontal component, so there is no compaction resistance in this section. According to Equation (26), the factors affecting the compaction resistance include the width and radius of the flexible wheel, the entry angle, the exiting angle, the deformation of the flexible wheel, and the normal stress of the circular arc section, and so forth, and the normal stress is related to the sinkage and lunar soil parameters.

When the rover is running, a large amount of lunar soil will be pushed in front of the wheel, which will cause bulldozing resistance, especially when the wheel is wide. On the basis of the passive earth pressure theory, the bulldozing resistance can be expressed as (Cardile et al., 2012)

$$R_b = \frac{B\sin(\theta_1 + \phi)}{2\sin\theta_1\cos\phi}\left[2z_e cK_c + \gamma z_e^2 K_\gamma\right] + \frac{\pi l^3\gamma(90 - \phi)}{540} + \frac{c\pi l^2}{180} + cl^2\tan\left(45 + \frac{\phi}{2}\right), \tag{27}$$

where K_c and K_γ are functions of the Terzaghi coefficient N_c and N_γ respectively, and l is the fracture length:

$$K_c = (N_c - \tan\phi)\cos^2\phi, \tag{28}$$

$$K_\gamma = \left(\frac{2N_\gamma}{\tan\phi} + 1\right)\cos^2\phi, \tag{29}$$

$$l = z_e \tan^2\left(45 - \frac{\phi}{2}\right). \tag{30}$$

As can be seen from Equation (27), the bulldozing resistance is affected by wheel width, friction angle of lunar soil, cohesion, bulk density, bearing coefficient, fracture length, and so forth. The fracture length l is related to wheel sinkage (affected by wheel width and radius). Intuitively, the bulldozing resistance increases with the increase in wheel width, and narrow wheels can significantly reduce the bulldozing resistance (Ellery, 2016; Gao et al., 2014). However, the increase in wheel width will reduce the sinkage and thus affect the resistance of bulldozing resistance. The influence of wheel width on bulldozing resistance is not a simple monotonically increasing relationship, so it is further analyzed in Section 3.2.

2.2.3 | Drawbar pull

Driving on the soft lunar terrain, the traction performance of the lunar rover is mainly limited by the shear characteristics between the wheel and the lunar soil. The thrust of lunar soil on wheels is determined by integrating the horizontal component of the shear stress on the contact interface using the shear stress formula described above:

$$H = Br\int_{\theta_c}^{\theta_1}\tau_1(\theta)\cos\theta\,d\theta + B\int_0^{l_{BC}}\tau_{BC}(\theta)\,dx + Br\int_{\theta_c}^{\theta_2}\tau_2(\theta)\cos\theta\,d\theta. \tag{31}$$

For a wheel with a tread, combined with the plastic balance theory, the lunar soil behind the wheel tread is in a passive failure state, and the horizontal thrust acting on the wheel tread is as follows:

$$F_p = B\left(\frac{1}{2}\gamma h_b^2 N_\phi + q h_b N_\phi + 2c h_b N_\phi\right), \tag{32}$$

$$N_\phi = \tan^2(45° + \phi/2), \tag{33}$$

where γ is the bulk density of the lunar soil, h_b is the lug height, N_ϕ is the bearing coefficient, q is the additional normal pressure acting on the surface of the lunar soil, c is the cohesion of the lunar soil, and ϕ is the interface friction angle of lunar soil.

Therefore, the resultant force of the thrust of the wheel carcasses and tread is

$$H_s = H + F_p. \tag{34}$$

The difference between the thrust and motion resistance of the lunar soil on the flexible wheel is the drawbar pull:

$$DP = H_s - \Sigma R, \tag{35}$$

where H_s is the resultant force of the thrust, ΣR is the motion resistance, which mainly includes compaction resistance R_c, and soil pushing resistance R_b.

2.2.4 | Torque

The driving torque T exerted by the lunar surface on the flexible wheel is determined by integrating the shear stress at the contact interface and multiplying the driving force by the corresponding moment arm, which is expressed as

$$T = Br^2\int_{\theta_c}^{\theta_1}\tau_1(\theta)\,d\theta + Br\cos\theta_c\int_0^{l_{BC}}\tau_{BC}(\theta)\,dx + Br^2\int_{-\theta_2}^{-\theta_c}\tau_2(\theta)\,d\theta. \tag{36}$$

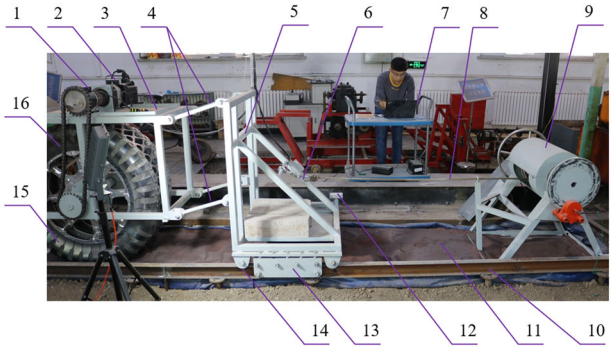

FIGURE 9 Soil bin test system. (1) Torque transducer, (2) motor reducer assembly, (3) main frames, (4) connecting rod, (5) trailer, (6) tension sensor, (7) computer, (8) tow rope, (9) drawbar pull control mechanism, (10) guide rail, (11) soil bin, (12) horizontal displacement sensor, (13) inhibiting device, (14) pulley, (15) flexible wheel, and (16) chain Transmission.

TABLE 1 Main technical parameters of the soil bin.

Parameter	Value
Soil bin dimension (mm)	9000 × 950 × 500 (length × width × height)
Diameter of the test wheel (mm)	800–1200
Width of the test wheel (mm)	<550
Maximum wheel load (N)	7500
Maximum rotational speed (rpm)	20
Maximum horizontal speed (m/min)	25
Slip ratio (%)	0–90

FIGURE 10 Bevameter.

TABLE 2 Parameters of the lunar soil simulant.

Parameters	JLU-M-1
n	1.03
k_c (kN/m^{n+1})	22.14
k_ϕ (kN/m^{n+2})	1438.5
c (kPa)	0.32
ϕ (°)	34.6
K (cm)	1.21
γ (g/cm^3)	1.87

3 | TRACTION PERFORMANCE PREDICTION

3.1 | Verification of the mathematical model

To verify the accuracy of the wheel soil interaction model, a large soil bin test system was developed. The soil bin test system is a necessary test equipment to study the wheel soil interaction. Its advantages are adjustable test parameters, high precision, low cost, short cycle, and so forth. In many studies at home and abroad, the interaction between wheel soil and soil has been studied by soil bin test (Jiang et al., 2017; Roozbahani et al., 2014; Tiwari et al., 2009; Yahya et al., 2007).

Figure 9 shows the soil bin test system. The whole system is mainly composed of a motor reducer, main frame, connecting rod, trailer, guide rail, soil tank, sensors, traction device, computer, and so forth. The wheel load can be adjusted by changing the counterweight on the main frame (1); the output torque of the motor reducer assembly (2) is measured by the torque sensor (3) and transmitted to the wheel axle by the chain drive (16); the connecting rod (4) is used to connect the main frame with the trailer (5) and ensure that the wheels can move freely in the vertical direction; the tension sensor (6) on the trailer is used to measure the drawbar pull, and the horizontal displacement sensor (12) is used to measure the horizontal displacement of the wheel and output to the computer to calculate the driving speed; the inhibiting device (13) and pulley (14) at the bottom of the trailer

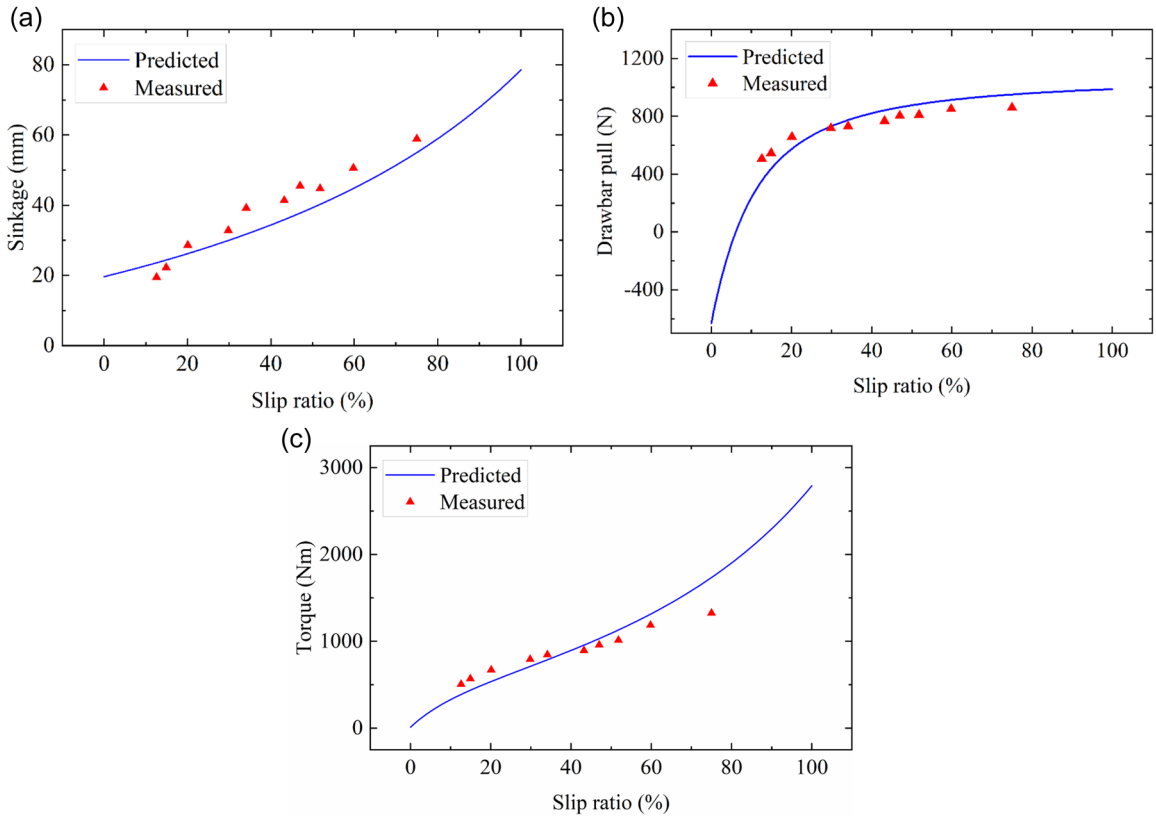

FIGURE 11 Comparison of theoretical and experimental results. (a) Sinkage, (b) drawbar pull, and (c) torque.

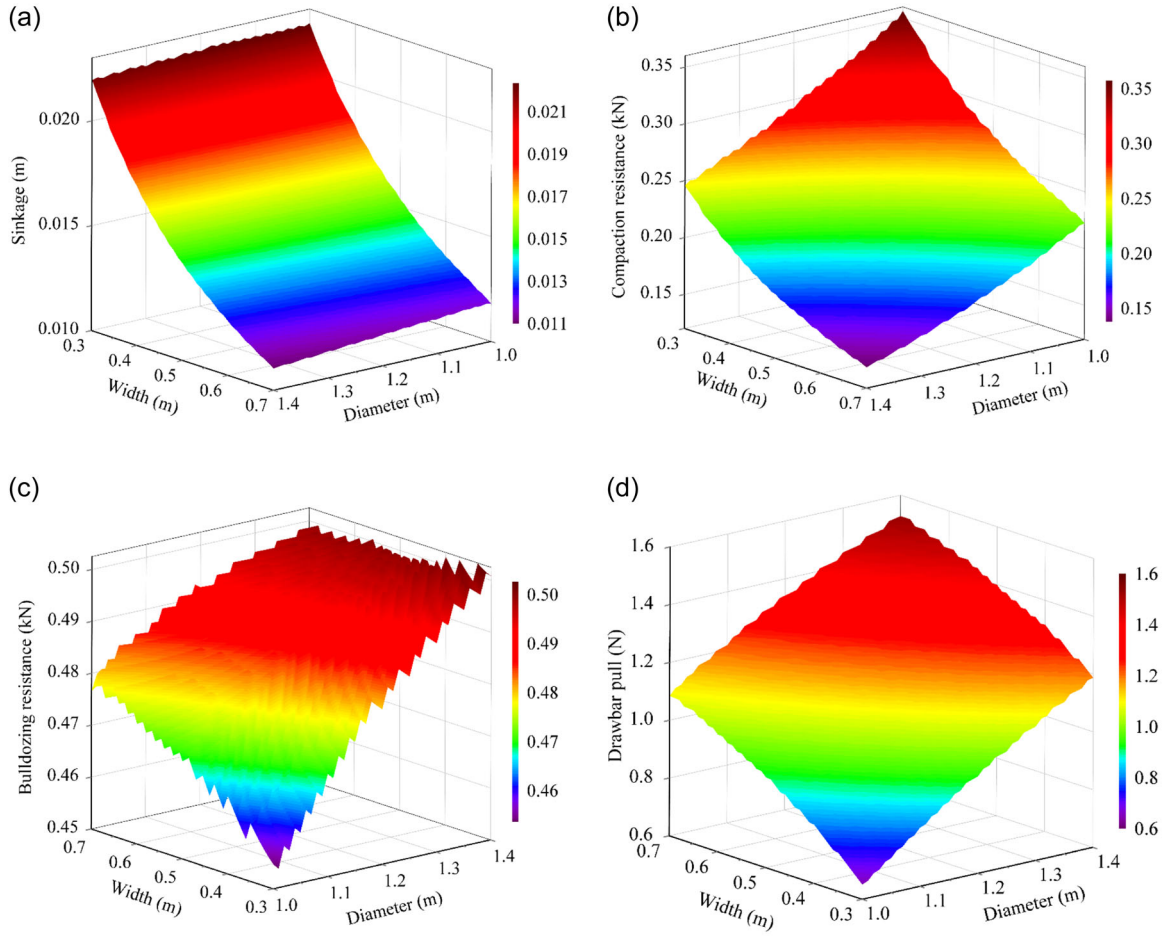

FIGURE 12 Influence of wheel width and diameter on traction performance. (a) Sinkage, (b) compaction resistance, (c) bulldozing resistance, and (d) drawbar pull.

are used to coordinate with the guide rails (10) to ensure that the test bed runs in a straight line. The main technical parameters of the soil bin test system are shown in Table 1.

To verify the accuracy of the wheel soil interaction model, soil bin tests were carried out using the soil bin test system. During the test, the wheel load was set as 4000 N, the driving speed was 0.12 m/s, and the lunar soil simulant was JLU-M-1. To measure the terramechanics properties of lunar soil simulant, a bevameter (Figure 10) was developed. The instrument can conduct two separate tests. One is the plate penetration tests and the other is the shear tests. In the penetration test, two round plates of different sizes were used and the pressure–sinkage relationship of the terrain is measured. In the shear tests, one shear plate was used to measure the shear stress–shear displacement relationship at various normal pressures. After data processing, the sinkage exponent n, cohesion modulus k_c, friction modulus k_ϕ, and shear deformation modulus K can be obtained. The parameters of the lunar soil simulant are listed in Table 2.

Figure 11 shows the comparison results between the theoretical results and the test results. Figure 11a shows that with the increase in slip ratio, the theoretical value and test value of sinkage gradually increase, and the average error between the theoretical value and test value is 13.9%. Figure 11b shows that with the increase in slip ratio, the theoretical and test value of the drawbar pull also gradually increases. When the slip ratio exceeds 60%, the drawbar pull tends to be flat, and the average error between the theoretical and the test results is 11.5%. Figure 11c shows that with the increase in slip ratio, the theoretical and test value of the torque increases gradually, the average error between the theoretical and the test results is 14.8%. When the slip ratio exceeds 60%, the error begins to increase. The above results show that although there is a certain error between the theoretical and the experimental results, the theoretical result can better reflect the changing trend of the traction performance and has high accuracy.

3.2 | Influence of wheel width and diameter on traction performance

To study the influence of wheel width and diameter on the traction performance of the flexible wheel, numerical analysis was conducted using the established wheel soil interaction model, as shown in

Figure 12. The wheel load was set as 3750 N, and the driving speed was 0.12 m/s.

Figure 12a shows the influence of wheel width B and diameter D on wheel sinkage z. It can be seen from the figure that the sinkage increase gradually decreases with the increase of wheel width and diameter, and the influence of wheel width on the sinkage is more significant than that of diameter. Therefore, the sinkage can be reduced by increasing the width and diameter of the flexible wheel.

Figure 12b shows the influence of flexible wheel width B and diameter D on compaction resistance. It can be seen from the figure that the compaction resistance decreases with the increase of the wheel width and diameter, and the influence of the wheel width on the compaction resistance is slightly greater than the diameter. Similarly, the compaction resistance of the wheel can be reduced by increasing the width and diameter of the flexible wheel appropriately.

Figure 12c shows the influence of wheel width B and diameter D on the bulldozing resistance. It can be seen from the figure that the bulldozing resistance increases gradually with the increase in wheel width. With the increase in diameter, the bulldozing resistance gradually decreases, which is more obvious when the diameter and width are smaller.

Figure 12d shows the influence of wheel width B and diameter D on the drawbar pull. It can be seen from the figure that the drawbar pull increases with the increase of the wheel width and diameter.

The above analysis shows that increasing the wheel diameter can effectively reduce the sinkage, compaction resistance, and bulldozing resistance, and increase the drawbar pull. However, increasing the wheel width can significantly reduce the sinkage and compaction resistance, and increase the drawbar pull. Therefore, when designing the flexible wheel, it can be considered to increase the width and diameter of the wheel appropriately to improve the traction performance of the flexible wheel.

4 | CONCLUSIONS

In this paper, a metal flexible wheel soil interaction model for a pressurized lunar rover was established, and the traction performance of the flexible wheel was predicted by using this model. When the flexible wheel is subjected to vertical load, the wheel carcasses will undergo elastic deformation in the wheel soil contact area. The load–deformation equation of the flexible wheel is obtained by the load–deformation test, which is used to predict the deformation of the flexible wheel. In this work, the deformation of the flexible wheel is divided into three sections and the wheel–soil interaction is calculated in sections. In this paper, the unique discrete wheel carcass structure makes the actual wheel soil contact area smaller than the nominal contact area. To improve the accuracy of the mathematical model, the wheel width is corrected to B^*. A numerical iterative method is proposed to solve the static sinkage and the entrance angle, and the dynamic interaction model is further solved according to the dynamic sinkage equation.

The accuracy of the wheel soil interaction model was verified by the soil bin test. The experimental results of the soil bin test showed that the average error between the theoretical value of sinkage and the experimental value was 13.9%, and the average error between the theoretical and experimental value of drawbar pull was 11.5%, indicating that the model has high prediction accuracy.

By analyzing the influence of different widths and diameters on the traction performance, it is found that increasing the wheel diameter can effectively reduce the sinkage, compaction resistance, and bulldozing resistance, while increasing the drawbar pull. However, increasing the wheel width can significantly reduce the sinkage and compaction resistance, while increasing the hook traction. Therefore, when designing the flexible wheel, it can be considered to increase the width and diameter to improve the traction performance.

It is found that the wheel tread has a significant influence on the traction performance of the flexible wheel. However, only one type of wheel tread is designed in this paper, and the influence of different types of wheel tread on traction performance will be further studied in the later work.

NOMENCLATURE

B	wheel width
B^*	equivalent wheel width
c	cohesion
DP	drawbar pull
F_1	supporting force on the part AB
F_2	supporting force on the part CD
F_c	supporting force on the part BC
F_p	thrust of tread
F_z	vertical reaction force
H	thrust
h_b	lug height
H_s	the resultant force of the thrust
i	slip ratio
j_{AB}	shear displacement of section AB
j_B	shear displacement at point B
j_{CD}	shear displacement of section CD
j_x	shear displacement at a distance x from point B
k	shear deformation modulus
K	shear deformation modulus
k_c	cohesive modulus
K_c	modulus of cohesion
K_γ	modulus of the density of soil deformation
k_ϕ	frictional modulus
l	fracture length
l_t	length of part BC
n	sinkage exponent
N_c	Terzaghi's bearing capacity factors
N_γ	Terzaghi's bearing capacity factors
N_ϕ	bearing coefficient
p_c	carcass stiffness
P_g	average ground pressure
$_{pi}$	inflation pressure
q	additional normal pressure

r	wheel radius
R_b	bulldozing resistance
R_c	compaction resistance
ΣR	motion resistance
T	driving torque
v	linear velocity
W	vertical load
W_1	vertical load on the test machine
z	sinkage of rigid wheel
z_1	sinkage at any point in section *AB*
z_2	sinkage at any point in section *CD*
z_c	sinkage of section *BC*
z_e	sinkage of flexible wheel
z_e'	slip sinkage

GREEK SYMBOLS

δ	deformation
γ	bulk density of the lunar soil
λ	equivalent coefficient
ω	angular velocity
ϕ	interface friction angle
σ	normal stress
σ_1	the normal stress of part *AB*
σ_2	the normal stress of part *CD*
σ_{BC}	the normal stress of part *BC*
τ	shear stress
τ_1	shear stress of part *AB*
τ_2	shear stress of part *CD*
τ_{BC}	shear stress of part *BC*
θ	contact angle
θ_1	entry angle
θ_2	exiting angle
θ_c	the contact angle for half of the flat section *BC*

ACKNOWLEDGMENTS

The authors thank the reviewers for their critical and constructive review of the manuscript. This work was supported by the National Natural Science Foundation of China (Grant Nos. 52075217 and 51775233), the Guangdong Aerospace Research Academy Research Project (Grant No. GARA2022003000), the Youth Innovation Promotion Association of the Chinese Academy of Sciences (Grant No. Y2022009) and the Experiments for Space Exploration Program and the Qian Xuesen Laboratory, China Academy of Space Technology (Grant No. TKTSPY-2020-05-01).

CONFLICT OF INTEREST STATEMENT

The authors declare no conflict of interest.

DATA AVAILABILITY STATEMENT

The data that support the findings of this study are available on request from the corresponding author. The data are not publicly available due to privacy or ethical restrictions.

ORCID

Meng Zou http://orcid.org/0000-0003-0498-4791

REFERENCES

Asnani, V., Delap, D. & Creager, C. (2009) The development of wheels for the lunar roving vehicle. *Journal of Terramechanics*, 46(3), 89–103.

Bekker, M.G. (1956) *Theory of land locomotion*. Ann Arbor: University of Michigan Press.

Bekker, M.G. (1960) Off-the-road locomotion. In: *Research development in terramechanics*. Ann Arbor: University of Michigan Press.

Bekker, M.G. (1969) *Introduction to terrain-vehicle systems. Part i: the terrain. Part ii: the vehicle*. Ann Arbor, Michigan: The University of Michigan Press.

Cardile, D., Viola, N., Chiesa, S. & Rougier, A. (2012) Applied design methodology for lunar rover elastic wheel. *Acta Astronautica*, 81(1), 1–11.

Ding, L., Deng, Z., Gao, H., Tao, J., Iagnemma, K.D. & Liu, G. (2015) Interaction mechanics model for rigid driving wheels of planetary rovers moving on sandy terrain with consideration of multiple physical effects. *Journal of Field Robotics*, 32(6), 827–859.

Ellery, A. (2016) *Planetary rovers*. Berlin: Springer.

Favaedi, Y., Pechev, A., Scharringhausen, M. & Richter, L. (2011) Prediction of tractive response for flexible wheels with application to planetary rovers. *Journal of Terramechanics*, 48(3), 199–213.

Gao, Q., Gao, F., Tian, L., Li, L., Ding, N., Xu, G. et al. (2014) Design and development of a variable ground clearance, variable wheel track self-leveling hillside vehicle power chassis (V2-HVPC). *Journal of Terramechanics*, 56, 77–90.

Gromov, V., Kemurdjian, A., Bogatchev, A., Koutcherenko, V., Malenkov, M. & Matrossov, S. et al. (2003) Lunokhod 2—a retrospective glance after 30 years. In: *Presented at the EGS-AGS-EUG Joint Assembly, held in Nice, France, 6–11 April, 2003*.

Guo, J., Li, W., Ding, L., Guo, T., Gao, H., Huang, B. et al. (2020) High-slip wheel–terrain contact modelling for grouser-wheeled planetary rovers traversing on sandy terrains. *Mechanism and Machine Theory*, 153, 104032.

Huang, H., Xu, S., Meng, Z., Li, J. & Zhang, J. (2018) The sinkage characteristics and prediction of a planetary rover based on a similarity model experiment. *Proceedings of the Institution of Mechanical Engineers, Part G: Journal of Aerospace Engineering*, 233(10), 3762–3774.

Huang, H., Xu, S., Wu, W., Zou, M., Zhang, J. & Li, J. (2019) Nonparametric terrain estimation for planetary rovers based on noncontact rut measurement. *Journal of Aerospace Engineering*, 32(2), 04018157. https://doi.org/10.1061/(ASCE)AS.1943-5525.0000986

Iizuka, K. & Kubota, T. (2011) Running performance of flexible wheel for lunar rovers on loose soil. *International Journal of Social Robotics*, 4(S1), 39–47.

Inotsume, H., Moreland, S., Skonieczny, K. & Wettergreen, D. (2019) Parametric study and design guidelines for rigid wheels for planetary rovers. *Journal of Terramechanics*, 85, 39–57.

Irani, R.A., Bauer, R.J. & Warkentin, A. (2011) A dynamic terramechanic model for small lightweight vehicles with rigid wheels and grousers operating in sandy soil. *Journal of Terramechanics*, 48(4), 307–318.

Janosi, Z. (1961) The analytical determination of drawbar pull as a function of slip for tracked vehicles in defarmable soils. In: *Proceedings of the 1st International Conference of ISTVS, Turin, 1961, Torino, Italy*.

Jiang, M., Dai, Y., Cui, L. & Xi, B. (2017) Soil mechanics-based testbed setup for lunar rover wheel and corresponding experimental investigations. *Journal of Aerospace Engineering*, 30(6), 06017005. https://doi.org/10.1061/(ASCE)AS.1943-5525.0000782

Kwan, C. (2021) A brief review of some interesting Mars rover image enhancement projects. *Computers*, 10(9), 111.

Lakdawalla, E. (2018) *The design and engineering of Curiosity: how the Mars Rover performs its job*. Berlin: Springer.

Li, C., Wang, C., Wei, Y. & Lin, Y. (2019) China's present and future lunar exploration program. *Science*, 365(6450), 238–239.

Lyasko, M. (2010) Slip sinkage effect in soil–vehicle mechanics. *Journal of Terramechanics*, 47(1), 21–31.

Poletayev, A.F. (1964) The compaction of soil under a rolling wheel. *Journal of Terramechanics*, 1(3), 7–17.

Reece, A.R. (1964) *Problems of soil vehicle mechanics*. Warren, MI: Army Tank-Automotive Center.

Reece, A.R. (1965) Principles of soil-vehicle mechanics. *Proceedings of the Institution of Mechanical Engineers: Automobile Division*, 180(1), 45–66.

Reeves, G. & Neilson, T. (2005) The Mars rover spirit FLASH anomaly. In: *2005 IEEE Aerospace Conference*. Big Sky, MT, USA: IEEE.

Roozbahani, A., Mardani, A., Jokar, R. & Taghavifar, H. (2014) Evaluating and measuring the performance parameters of agricultural wheels. *International Journal of Agricultural Biosystems Engineering*, 7(2), 158–162.

Sharma, G., Tiwary, S., Kumar, A., Suresha Kumar, H.N. & Keshava Murthy, K.A. (2018) Systematic design and development of a flexible wheel for low mass lunar rover. *Journal of Terramechanics*, 76, 39–52.

Squyres, S. (2005) *Roving Mars: spirit, opportunity, and the exploration of the red planet*. Hachette UK: Hyperion.

Sutoh, M., Nagaoka, K., Nagatani, K. & Yoshida, K. (2013) Design of wheels with grousers for planetary rovers traveling over loose soil. *Journal of Terramechanics*, 50(5–6), 345–353.

Sutoh, M., Yusa, J., Ito, T., Nagatani, K. & Yoshida, K. (2012) Traveling performance evaluation of planetary rovers on loose soil. *Journal of Field Robotics*, 29(4), 648–662.

Tiwari, V.K., Pandey, K.P. & Sharma, A.K. (2009) Development of a tyre traction testing facility. *Journal of Terramechanics*, 46(6), 293–298.

Wan, W.X., Wang, C., Li, C.L. & Wei, Y. (2020) China's first mission to Mars. *Nature Astronomy*, 4(7), 721.

Wang, S., Zou, M., Dang, Z., Chen, B., Zhou, T. & Su, B. (2019) Modelling of flexible metal wheels for planetary rover on deformable terrain. *Thin-Walled Structures*, 141, 97–110.

Wiberg, V., Servin, M. & Nordfjell, T. (2021) Discrete element modelling of large soil deformations under heavy vehicles. *Journal of Terramechanics*, 93, 11–21.

Wong, J.Y. (2009) *Terramechanics and off-road vehicle engineering: terrain behaviour, off-road vehicle performance and design*. Oxford, UK: Butterworth-Heinemann.

Wong, J.-Y. & Reece, A.R. (1967a) Prediction of rigid wheel performance based on the analysis of soil–wheel stresses. Part II. Performance of towed rigid wheels. *Journal of Terramechanics*, 4(2), 7–25.

Wong, J.-Y. & Reece, A.R. (1967b) Prediction of rigid wheel performance based on the analysis of soil–wheel stresses. Part I. Performance of driven rigid wheels. *Journal of Terramechanics*, 4(1), 81–98.

Yahya, A., Zohadie, M., Ahmad, D., Elwaleed, A.K. & Kheiralla, A.F. (2007) UPM indoor tyre traction testing facility. *Journal of Terramechanics*, 44(4), 293–301.

Zou, M., Zhu, J., Wang, K., Lin, Y., Jin, J. & He, L. et al. (2020) Design and mechanical behavior evaluation of flexible metal wheel for crewed lunar rover. *Acta Astronautica*, 176, 69–76.

How to cite this article: Zhu, J., Shen, Y., Hao, P., Liu, J., Li, Y., Wang, K. & Zou, M. (2023) Modeling of Flexible Metal Wheel for Pressurized Lunar Rover and Traction Performance Prediction. *Journal of Field Robotics*, 40, 2030–2041. https://doi.org/10.1002/rob.22239